AIAA 95-0033

N15

FLOW CHARACTERISTICS IN BOUNDARY LAYER BLEED SLOTS WITH PLENUM

NAG 3-1213
IN-34-CR
Overrode
5580

A. Hamed*, J.J. Yeuan and Y.D. Jun*****
Department of Aerospace Engineering and Engineering Mechanics
University of Cincinnati
Cincinnati, OH 45221

p. 10

Abstract

Numerical simulations were conducted to investigate the performance characteristics of bleed through normal slots and its effect on the turbulent boundary layer development under zero and strong adverse pressure gradient caused by incident oblique shock. The solution to the compressible Navier-Stokes and k-ε equations was obtained in a domain that includes the regions inside the bleed slot and plenum in addition to the external flow. The computational results demonstrate the interactions between the plenum, and bleed flow and the effect of incident shock on the boundary layer development downstream. The computed results agree with the experimentally measured pitot and static pressure distribution inside the slot. The bleed mass flow without incident shock was underpredicted over the range of plenum pressures. The computations predicted the measured increase in bleed mass flow with incident shock.

Introduction

Bleed is used in supersonic inlets to control the effects of flow separation associated with shock boundary layer interactions on ramps, cowls and side walls. In order to predict the effect of bleed on the boundary layer development and internal shock structure, few investigators [1-3] included ramp chambers, throat plenum and exit louvers in their supersonic inlet flow simulations. However, because of the enormous increase in computational time and grid generation complexity, most investigators simulated the global effects of bleed by changing the boundary conditions [4-7] and/or the turbulence models [8,9] in the bleed regions. The imposed mass flux in the bleed area was based on experimental measurements in some investigations [7] and on empirical correlation of the bleed discharge coefficient in others [4-6]. Even when the turbulence model was modified for mass removal at the porous wall [8] the effect of bleed on boundary layer development was not adequately predicted.

Reproducing the experimentally measured boundary layer profiles over the porous wall even required the implementation of blowing rather than suction in the turbulence model [8]. Paynter et al. [9] used a rough wall algebraic turbulence model to simulate the increase in the growth rate of boundary layer induced by bleed, by changing the roughness parameter in the numerical solutions to the Navier-Stokes equations until the boundary layer profiles matched the experimental measurements [10, 11]. They determined that roughness was a strong function of the upstream boundary layer mass flux removed, in the bleed rates between 3% and 15%. However Paynter et al. pointed out that the experimental set-up whose data they used to develop their model, may have produced non uniformity in the mean velocity distribution and nonequilibirum boundary layer in the bleed region. In general, bleed models are restricted by the particular flow conditions and any inadequacies in the experimental data used in their model development. According to Hamed and Shang [12], the conclusions regarding the effects of bleed hole size and bleed location relative to the shock were not consistent among several experimental studies.

Hamed, et al. [13-18] and Remlinger, Shih and Chyll [19-22] followed an alternative approach to investigating bleed effects. They conducted numerical simulations in which the viscous flow field was resolved inside the individual bleed holes and slots. This approach helps in understanding the important local phenomena that control the flow in the bleed regions, and how they are affected by the bleed configuration, and the external flow conditions. These type of investigations can and have been used in simple flow configurations to study the relative effects of bleed/slot angle, size and location. They revealed the presence of a separation bubble near the hole/slot entrance and a "bleed shock" that initiates inside the hole/slot and attaches to the downstream corner under certain conditions. The size of the separation bubble which controls the bleed discharge coefficient is strongly affected by bleed hole/slot slant angle and less by the free stream

* Professor, Fellow AIAA.
** Post Doctoral Assistant, Member AIAA.
*** Student Member, AIAA.

conditions and plenum pressure. The boundary layer development downstream was strongly influenced by the bleed angle and the bleed shock strength.

The purpose of present numerical study is to investigate the effects of external flow and plenum conditions on bleed performance. In the investigated configuration bleed is applied to a flat plate turbulent boundary layer through a normal slot. The numerical solution to the viscous flow inside the slot and plenum and over the plate surface were obtained for supersonic flow with and without impinging shock at the slot's upstream corner. The flow computations were conducted over a range of plenum pressures up to choked bleed conditions. The results, which are compared with experimental data, show the flow characteristics inside the bleed slot and the effect of bleed on the boundary layer development downstream with and without incident shock.

Flow Configuration and Computational Details

In the investigated flow configuration shown schematically in Fig. 1, bleed is applied through a normal slot to the turbulent boundary layer on a flat plate. The bleed slot whose width is one centimeter and its depth 2.54 cm is connected to a 41.4 cm x 63.5 cm plenum. Outside of the slot, the solution domain extended 12.2 cm above and 40.9 cm along the flat plate surface. The boundaries AB and CD were located at 28.2 cm upstream and 12.7 cm downstream of the slot's upstream corner to match the locations of experimental velocity profile measurements in reference [6].

The flow computations were conducted using the PARC code [23] with the compressible k-ε turbulence model of Chien [24] modified by Nichols [25] for compressibility effects. The change in bleed mass flow rate was achieved through changing the static pressure at the plenum's outflow boundary. Referring to Fig. 1, the upstream boundary conditions consisted of free stream Mach number, stagnation pressure and stagnation temperature and a computed boundary layer velocity profile for flat plate computations which was matched to the experimentally measured profile's displacement and momentum thickness. The pre-shock and post-shock conditions were specified along the upper boundary to locate the inviscid incident shock at the upstream corner of the slot and flat plate surface. Flow variables were extrapolated at the downstream boundary and at the plenum's outflow boundary where the static pressure was specified to control the bleed mass flow. The initial conditions were specified from the solution without bleed for a given free stream Mach number. Subsequently, the computed flow field with the bleed slot and plenum was used to initialize the solutions at higher bleed mass flow rates (lower plenum pressure settings).

The computational grid shown in Fig. 2 includes a 308x68 grid over the flat plate surface, 89x68 grid inside the bleed slot and 187x148 grid inside the plenum chamber. Variable grid spacing was used in both x and y directions for grid clustering around the bleed walls, plenum chamber walls and at the plate surface, with $x_{min} = 0.9446 \times 10^{-3}$ cm and $y_{min} = 0.4755 \times 10^{-3}$ cm corresponding to $y^+ = 0.959$ at the inflow turbulent boundary layer at 2.46 free stream Mach number.

Results and Discussion

Typical results of the computed flow inside the slot near choked conditions are presented in Fig. 3 and compared with the experimental results of Davis et al. [27] reproduced in Figures 4 for incident oblique shocks whose inviscid impact point coincides with the slot's upstream corner at x=0. The figures present the pitot and static pressure contours for a shock generation angle $\alpha = 8°$, at 2.46 free stream Mach number. The computations predict very well both the shape and magnitude of the pressure contours inside the slot, the location of flow separation, and the size of the separation bubbles on the slot walls. The computed Mach number and velocity vectors, which are shown in Fig. 5, indicate flow angles of 33° from the plate surface, and high Mach numbers of 1.8 in a triangular region at the center of the slot opening. Disagreements can be observed between the experimental and computational results in this region. Since the pitot probe was always parallel to the slot walls in the experiment, one should expect discrepancies in these regions where the probe is oriented at 67° angle to the Mach 1.8 flow. The sharp gradients in the pressure across "bleed shock" were also not resolved by the measurements. The experiment indicates reattachment of the flow on the slot's downstream wall near the exit, which was not predicted by the computations.

Effect of Incident Shock

The effect of incident shock at the slot's upstream corner is demonstrated by comparing the computational results with and without the shock. Figures 6 and 7 present the computed Mach number and pressure contours inside the slot and in the neighboring regions over the plate surface and inside the plenum. The Mach number contours inside the slot indicate that when there is no incident shock, the separated flow region along the slot's upstream wall is much larger while the separated flow region over the slot's downstream wall near the exit is much smaller. In addition, the Mach number contours indicate less flow turning into the slot when there is no incident shock. This coincides with a weaker expansion fan at the slot's upstream corner as can be seen from the pressure contours. Also without incident shock, the "bleed shock" which originates inside the slot is quickly weakened outside

through interactions with a second expansion fan at the slot's downstream corner.

The maximum computed bleed mass flow with and without incident shock was 5.1% and 2.35% of the incoming boundary layer for the slot geometry (D/δ = 0.38). The pressure and Mach number contours indicate a separation bubble on the plate surface upstream of the slot in the case of incident shock. This is confirmed by the skin friction coefficient distribution of Fig. 8. One can see from Fig. 8 that there is a large difference in the predicted friction coefficients with and without incident shock within two slot widths downstream of bleed. In order to understand the cause of this difference, the mass flux, flow angle, and Mach number distribution across the slot opening are presented in Figs. 9-11. In the case of no incident shock, the mass flows out of the slot in the subsonic region behind the "bleed shock" and the downstream slot wall. This flow turns around the slot corner and forms the boundary layer over the plate surface. In the case of incident shock the subsonic flow goes into the slot opening in the region behind the "bleed shock", and the flow over the plate surface downstream originates outside the slot.

According to the velocity profiles of Fig. 12, the effect of incident shock is seen to extend over two to three slot widths upstream and downstream of the slot, where the distorted velocity profiles are less full near the plate. The distortion upstream is associated with the shock induced pressure gradient and flow separation. The shape of the profiles downstream is affected both by the local flow conditions above the slot and by the strength of the "bleed shock" at the slot opening. Since the incident shock reduces the flow velocity, the profiles downstream of the slot are less full near the wall. The "bleed shock", has smaller effect on the downstream velocity profiles in the case with no incident shock because it is quickly weakened by the expansion fan at the slot's downstream corner.

Plenum Interactions

A considerable part of the computational effort was consumed in modeling the flow field inside the plenum. The increased computational effort was not only associated with the number of grid points inside the plenum (50.6% of the total) but also with the slower convergence of the flow at low subsonic plenum speeds. In order to determine the nature of the plenum interactions with the bleed and external flow fields, the bleed mass flux was monitored at the slot opening (bleed inflow) and exit (bleed outflow) during the computations. Fluctuations persisted in the bleed mass at both inflow and outflow boundaries when the computations were conducted using local time stepping. The amplitude of the bleed mass flow fluctuations was higher at higher plenum pressures and diminished near choking. Subsequently one time accurate flow simulation was performed with α=8° incident shock at choked bleed conditions. The computational results indicated no fluctuations in the bleed mass flow at the slot's inflow boundary in this case and much smaller fluctuations in the bleed mass flow at the outflow boundary compared to the local time stepping results. Additional numerical computations with local time stepping were then performed without the plenum. The bleed mass flow in these computations did not fluctuate and coincided with the time accurate bleed mass flow at the slot's inflow boundary.

The discharge coefficient, Q, and the flow coefficient, F, are used to present the bleed mass flow data in nondimensional form. They are defined as follows:

$$Q = m_b / A_b P_r \left(\frac{\gamma}{RT_{t_{inf}}}\right)^{\frac{1}{2}} \left(\frac{2}{\gamma+1}\right)^{\frac{\gamma+1}{2(\gamma-1)}}$$

When the stagnation free stream value $P_{t_{inf}}$ is used for the reference pressure, P_r, the discharge coefficient, Q, represents the ratio between the bleed mass flow and the ideal mass flow that could pass into the slot at sonic conditions if the flow was to expand isentropically to fill the bleed area A_b. On the other hand, the flow coefficient represents the ratio between the bleed mass flow and the mass flow that would pass through the bleed area at the flow conditions $\rho_e U_e$ outside the boundary layer

$$F = m_b / A_b \rho_{inf} U_{inf}$$

The predicted variation in the discharge coefficient with plenum pressure is presented in Fig. 13 with the experimental results of references [26] and [27]. The figure shows the computed bleed mass flow without plenum, as well as the range of bleed mass flow fluctuations in the computations with plenum using local time stepping. The computations without plenum agree with the experimental data in the case of incident shock, but under-predict the bleed mass flow without shock over the range of plenum pressures. The much higher discharge coefficient in the case of incident oblique shock can be caused by the increased static pressure above the slot and/or the velocity distortion upstream. In order to separate the two effects, a bleed discharge coefficient based on the local static pressure, P_{loc}, is presented in Fig. 14. The value of the local static pressure was taken as P_{inf} for no incident shock and P_1, the inviscid static pressure behind the incident shock (P_1/P_{inf} = 1.7). This figure indicates that the difference in the computed discharge coefficient with and without incident shock becomes smaller based on this normalization. The remaining

difference can be attributed to the incoming velocity profile distortion by the incident shock.

Conclusions

Numerical simulations were conducted for supersonic flow at Mach 2.46, with bleed applied through a normal slot with and without incident shock at the slot's upstream corner. The computed results agree with the experimental measurements inside the slot in the case of incident shock. The computations indicate higher flow angles at the slot opening and a narrower separation bubble on the slot's upstream wall in the case of incident shock which leads to higher discharge coefficient. The "bleed shock" which originates inside the slot and extends as an oblique shock outside is quickly weakened in the case with no incident shock by the interactions with an expansion fan at the slot's downstream corner.

The plenum caused fluctuations in the bleed mass flux at the slot exit but time accurate computations at choked conditions indicated that these disturbances did not affect the flow and mass flux at the slot opening. The fluctuations were associated with the lateral movement of the bleed flow between the two separation bubbles on the slot walls. The computed bleed mass flow without plenum coincided with the predicted steady value at the slot inlet in the time accurate numerical simulations with plenum. The experimental data for bleed mass flow agreed with the computations in the case of incident shock but were higher with no incident shock.

Acknowledgements

This work was sponsored NASA Grant NAG3-1213, Dave Saunders, Project Monitor. The computational work was performed on the CRAY YMP of the Ohio Supercomputer.

References

1. Forester, C.K., and Tjonneland, E., "New Guide for Accurate Navier-Stokes Solution of Two-Dimensional External Compression Inlet with Bleed," International Council of the Aeronautical Sciences 88-2.5.1, 1988.

2. Fujimoto, A., Niwa, N., and Sawada, K., "Numerical Investigation on Supersonic Inlet with Realistic Bleed and Bypass Systems," AIAA Paper 91-0127,. Jan. 1991.

3. Fujimoto, A. and Niwa, N., "Experimental and Numerical Investigation of Mach 2.5 Supersonic Mixed Compression Inlet," AIAA 93-0289, January 1993.

4. Abrahamson, K.W., "Numerical Investigation of a Mach 3.5 Axisymmetric Inlet," AIAA 93-0289, January 1993.

5. Benhachmi, D., Greber, I. and Hingst, W., "Experimental and Numerical Investigation of an Oblique Shock-Wave/Turbulent Boundary Layer Interaction with Continuous Suction," AIAA Paper 89-0357, January 1989.

6. Saunders, J.D. and Keith, T.G., Jr., "Results from Computational Analysis of a Mixed Compression Supersonic Inlet," AIAA 91-2581, June 1991.

7. Reddy. D.R., Benson, t.J., and Weir, L.J., "Comparison of 3-D Viscous Flow Computations of March 5 Inlet with Experimental Data," AIAA Paper 90-0600, Jan. 1990.

8. Lee, D.B. and Leblanc, R., "Interaction onde de Choc Oblique-Couch Limite sur Paroi Poreuse avec Aspiration," Paper 23, AGARD CP-365, "Improvement of Aerodynamic Performance Through Boundary Layer Control and High Lift Systems," August 1984.

9. Paynter, G.C., Treiber, D.A. and Knelling, W.D., "Modeling Supersonic Inlet Boundary Layer Bleed Roughness," J. of Propulsion and Power, Vol. 9, No. 4, 1994, pp. 622-627.

10. Schuehle, A.L., "Tabulation of the Boundary Layer Profile Data Taken for the SST Bleed System Development and Performance Test," Boeing METM-70-50, August 26, 1970.

11. Mayer, D.W., "Turbulent Supersonic Boundary Layer Flow in an Adverse Pressure Gradient Including the Effects of Mass Bleed," MSME Thesis, University of Washington, 1977.

12. Hamed, A. and Shang, J., "Survey of Validation Data Base for Shock Wave Boundary Layer Interactions in Supersonic Inlets," Journal of Propulsion, Vol. 7, No. 4, July 1991, pp. 617-625.

13. Hamed, A., Shih, S. and Yeuan, J.J., "Investigation of Shock/Turbulent Boundary-Layer Bleed Interactions," Journal of Propulsion and Power, Vol. 10, No. 1, Jan.-Feb. 1994, pp. 79-87.

14. Hamed, A., Yeuan, J.J. Shih, S.H., "An Investigation of Shock Wave Turbulent Boundary-Layer Interaction with Bleed through Slanted Slots," AIAA Paper No. 93-2992, July 1993.

15. Hamed, A., Yeuan, J.J. and Shih, S.H., "An Investigation of Bleed Through Normal and Slanted Slots in Shock Wave Turbulent Boundary Layer Interaction," AIAA Paper No. 93-2155, June-July 1993.

16. Hamed, A.. Shih, S.H. and Yeuan, J.J., "A Parametric Study of Bleed in Shock Boundary Layer Interactions," AIAA Paper No. 93-0294, January 1993.

17. Hamed, A. and Lehnig, T., "Effect of Bleed Configuration on Shock/Laminar Boundary-Layer Interactions," *to appear in* J. of Propulsion & Power, Vol. 11, No. 1, Jan. Feb. 1995.

18. Hamed, A. and Lehnig, T., "Investigation of Oblique Shock/Boundary-Layer Bleed Interaction," J. of Propulsion and Power, Vol. 8, No. 2, March-April 1992, pp. 418-424.

19. Rimlinger, M.J., Shih, T.I-P and Chyu, W.J., "Three-Dimensional Shock-Wave/Boundary-Layer Interactions with Bleed Through Multiple Holes," AIAA Paper 94-0313, January 1994.

20. Shih, T.I-P, Rimlinger, M.J. and Chyu, W.J., "Three-Dimensional Shock-Wave/Boundary Layer Interactions with Bleed," AIAA Journal, Vol. 31, No. 10, 1993, pp. 1819-1826.

21. Chyu, W.J., Rimlinger, M.J. and Shih, T.I-P, "Effects of Bleed-Hole Geometry and Plenum Pressure on Three-Dimensional Shock-Wave/Boundary Layer/ Bleed Interactions," AIAA Paper 93-3259, July 1993.

22. Rimlinger, M.J., Shih, T.I-P and Chyu, W.J., "Three-Dimensional Shock-Wave/Boundary-Layer Interactions with Bleed Through a Circular Hole," AIAA Paper 92-3084, July 1992.

23. Cooper, G.K., and Sirbaugh, J.R., "PARC Code: Theory and Usage," AEDC-TR-89-15, 1989.

24. Chien, K-Y, "Prediction of Channel and Boundary-Layer Flows with a Low Reynolds Number Turbulence Model," AIAA Journal, Vol. 20, January 1982, pp 33-38.

25. Nichols, R. H., "A Two-Equation Model for Compressible Flows," AIAA Paper 90-0494, AIAA 28th Aerospace Sciences Meeting, Reno, NV, January 1990.

26. Willis, B., Davis, D. and Hingst, W., "Flow Coefficient Behavior for Boundary-Layer Bleed Holes and Slots," AIAA Paper 95-0031, 33rd Aerospace Sciences Meeting, Reno, Nevada, January 9-13, 1995.

27. Davis, D., Willis, B. and Hingst, W., "Flowfield Measurements in Slot-Bled Oblique Shock-Wave and Turbulent Boundary-Layer Interaction," AIAA Paper 95-0032, 33rd Aerospace Sciences Meeting, Reno, Nevada, January 9-13, 1995.

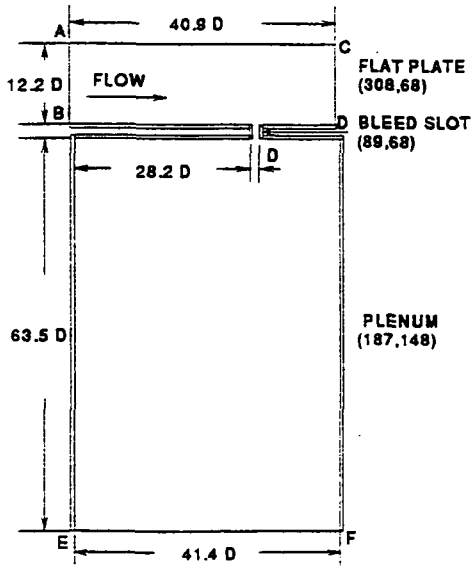

Fig. 1. Schematic of Computational Domain.

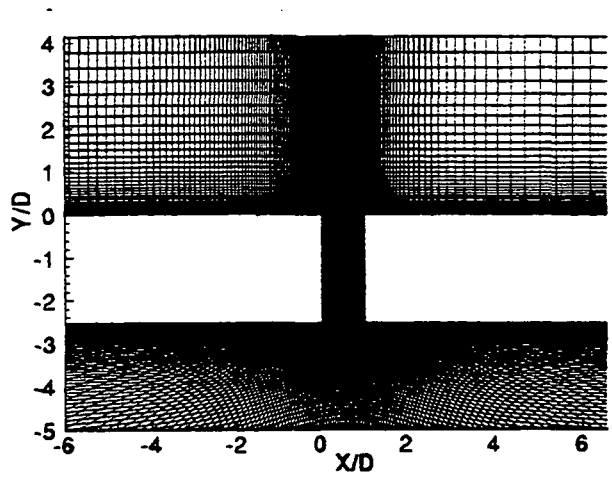

Fig. 2. Computational Grid Near Bleed Slot.

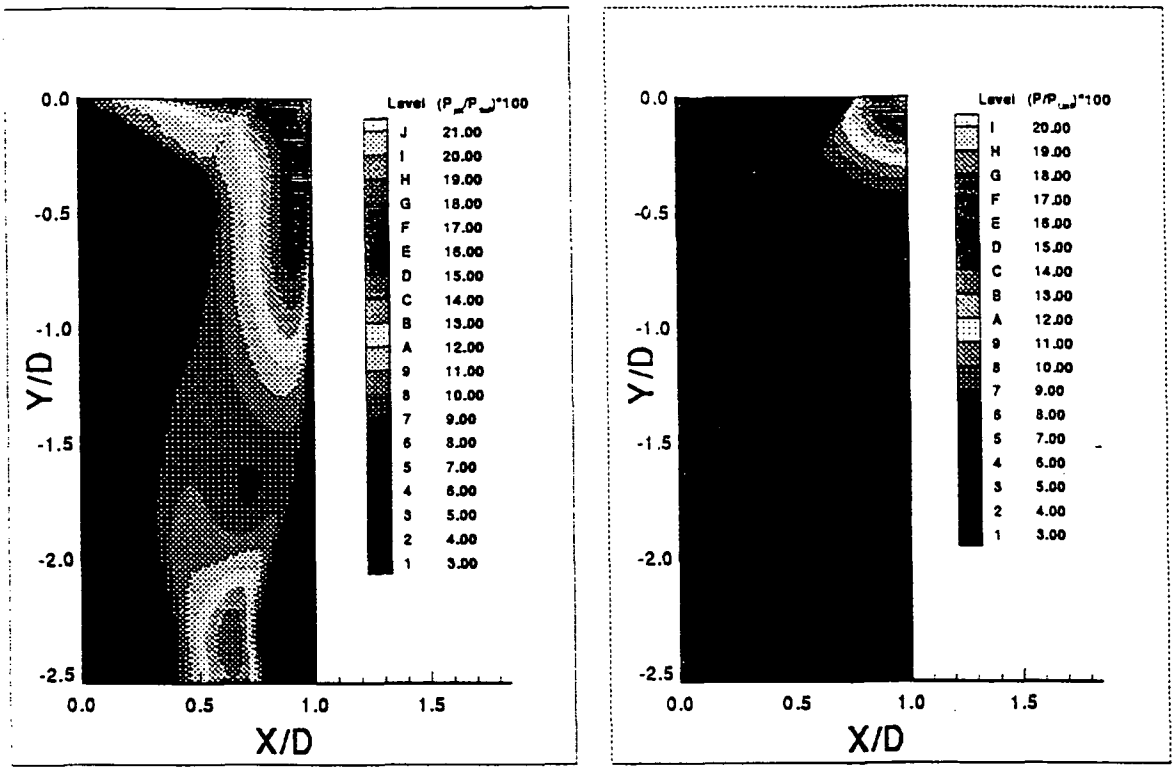

Fig. 3. Pitot and Static Pressure Contours Inside Slot
(Computational Results) M = 2.46, $\alpha = 8°$.

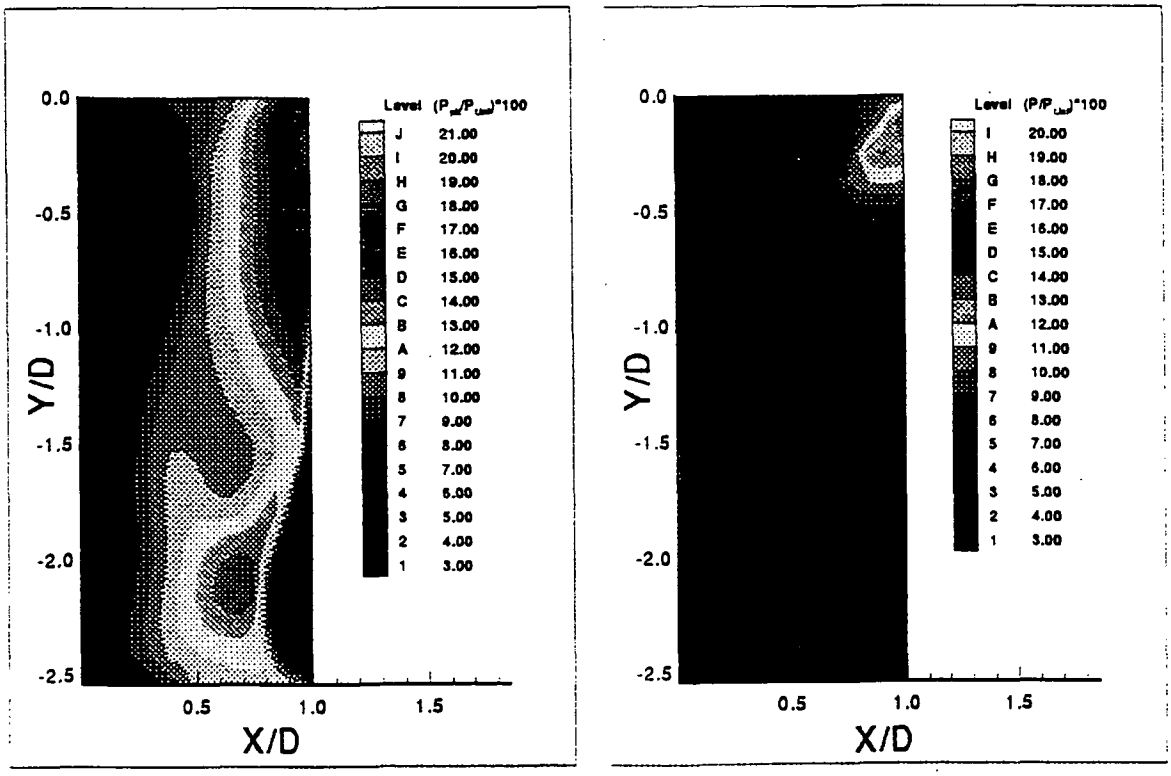

Fig. 4. Pitot and Static Pressure Contours Inside Slot
(Experimental Results [27]) M = 2.46, $\alpha = 8°$.

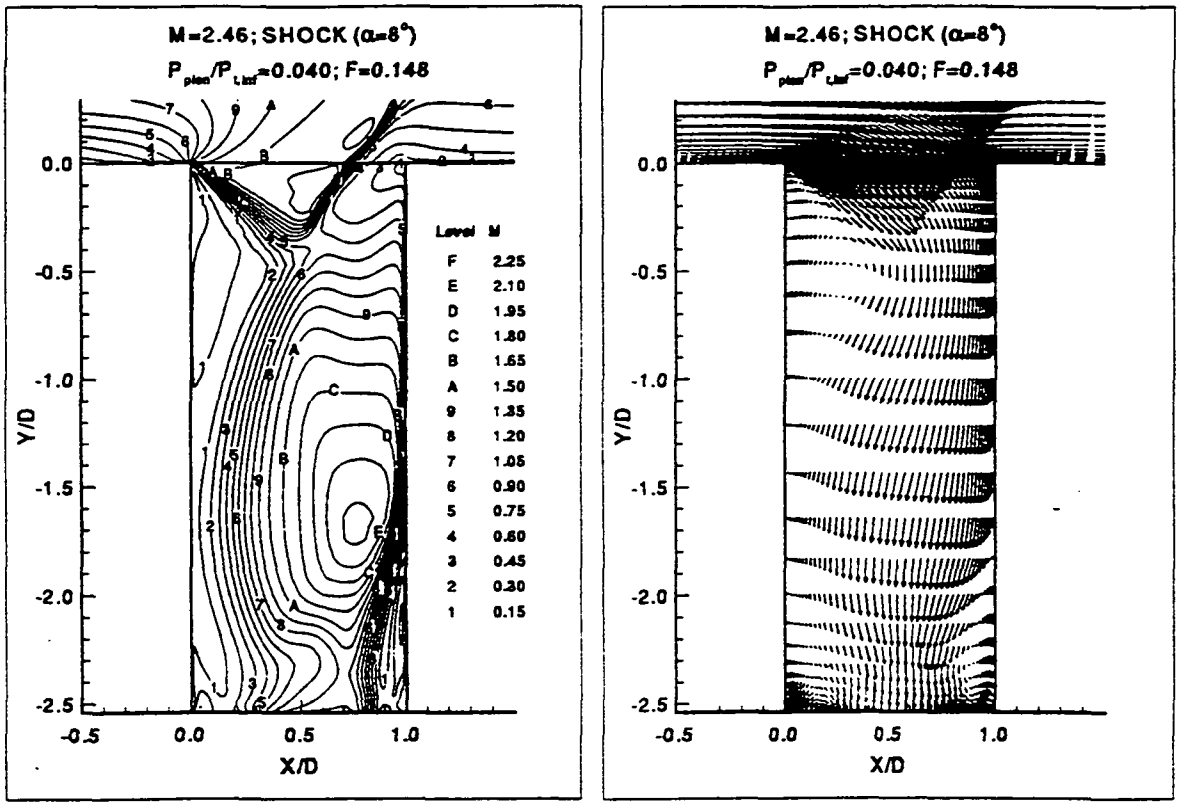

(a) Mach Number Contours (b) Velocity Vectors

Fig. 5. Velocity Field Inside Slot

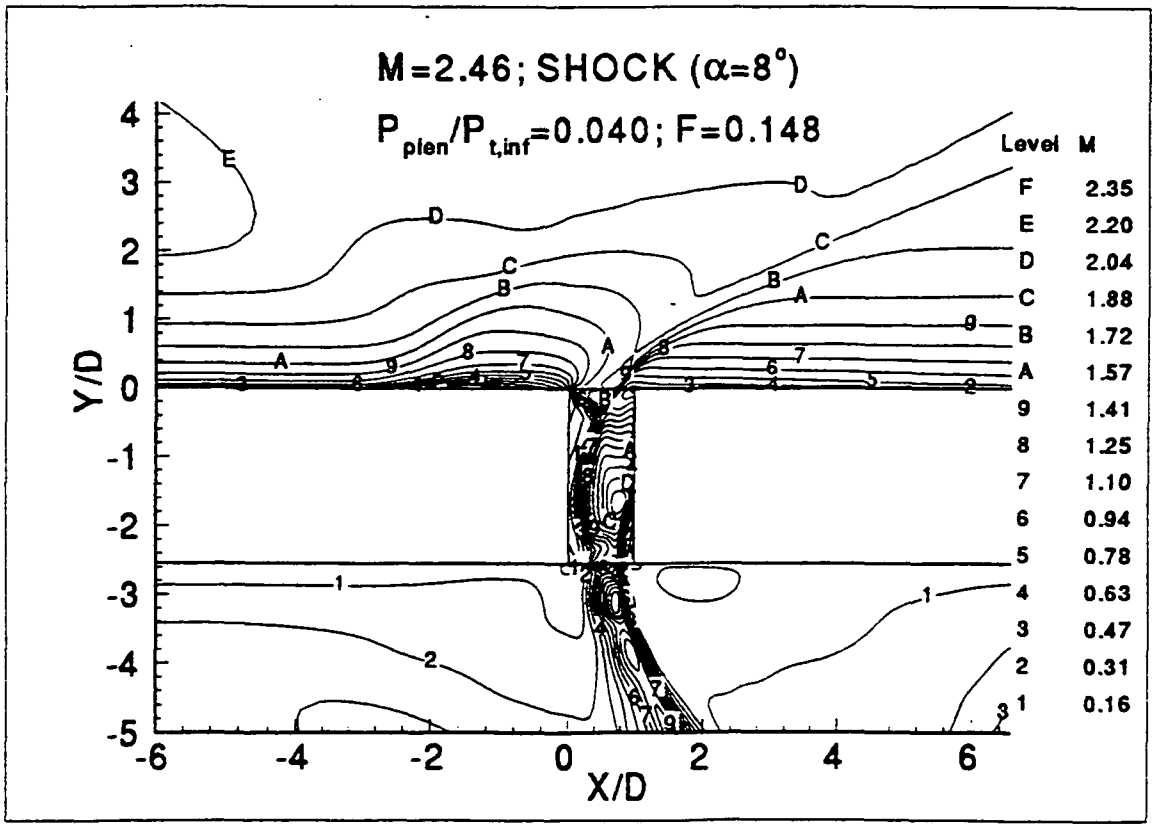

(a) With Incident Shock

Fig. 6. Comparison of the Mach Number Contours With and Without Incident Shock

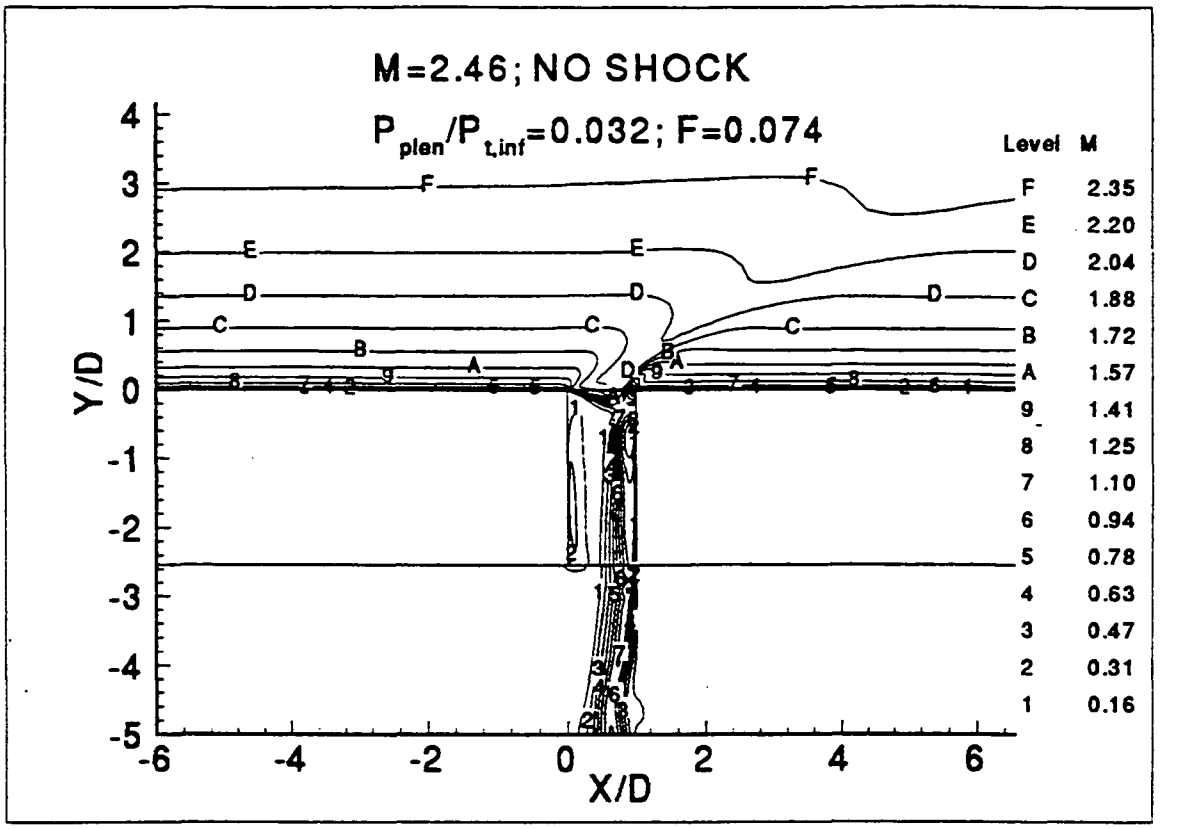

(b) Without Incident Shock

Fig. 6. Comparison of the Mach Number Contours With and Without Incident Shock

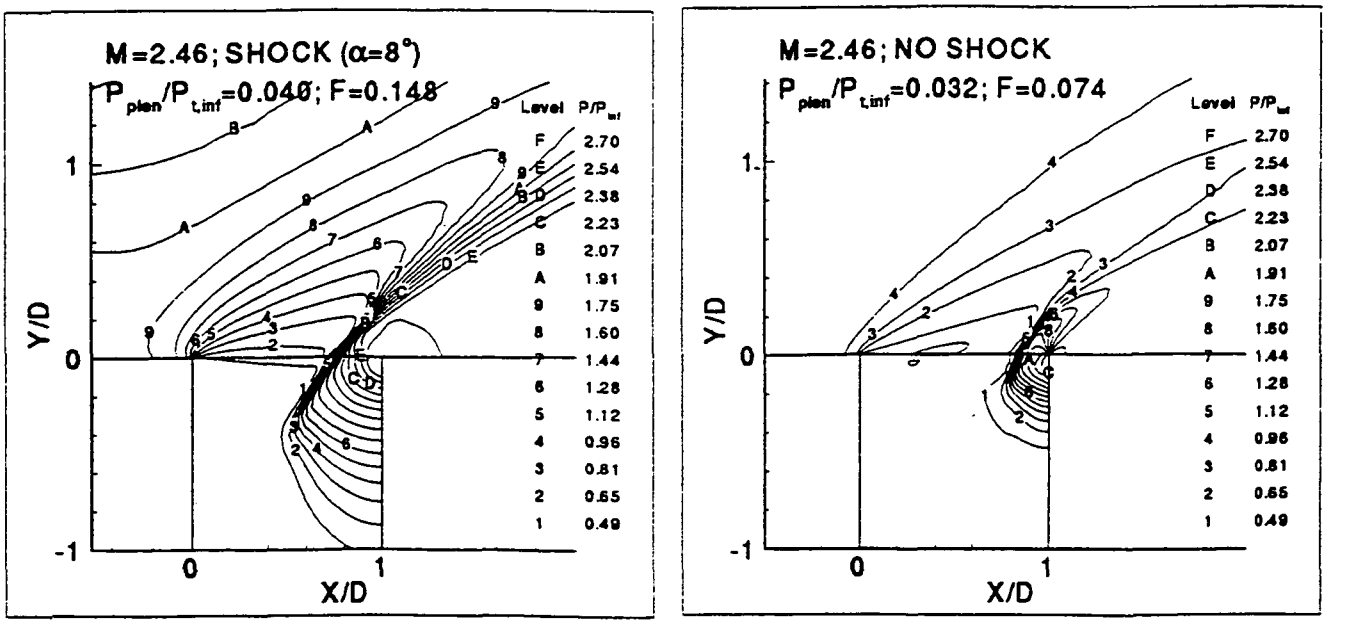

(a) With Incident Shock

(b) Without Incident Shock

Fig. 7. Comparison of the Pressure Contours With and Without Incident Shock

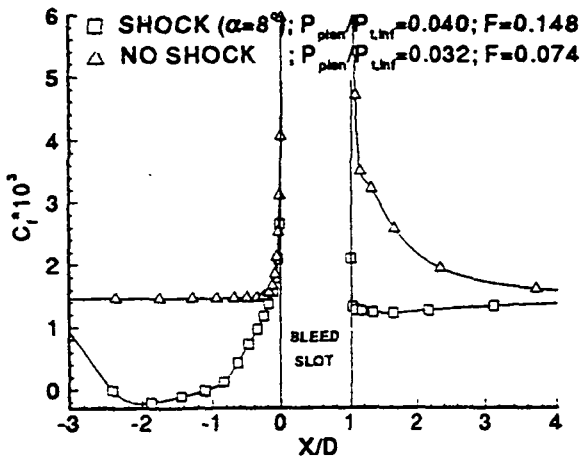

Fig. 8. Skin Friction on the Plate Surface.

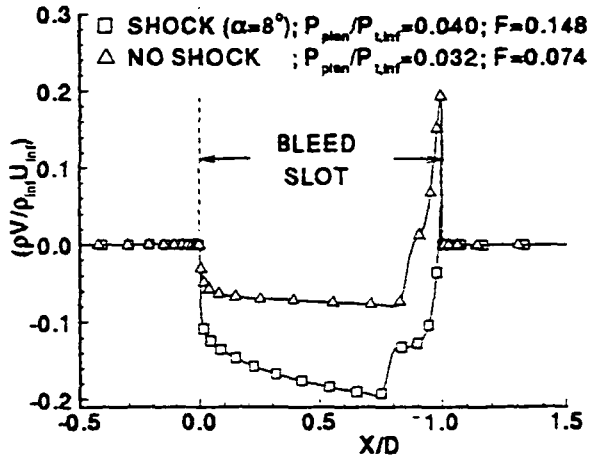

Fig. 9. Bleed Mass Flux Across Slot Opening

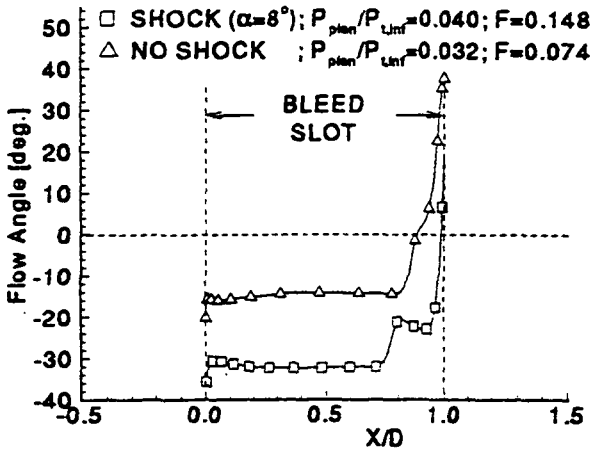

Fig. 10. Flow Angle Across Slot Opening.

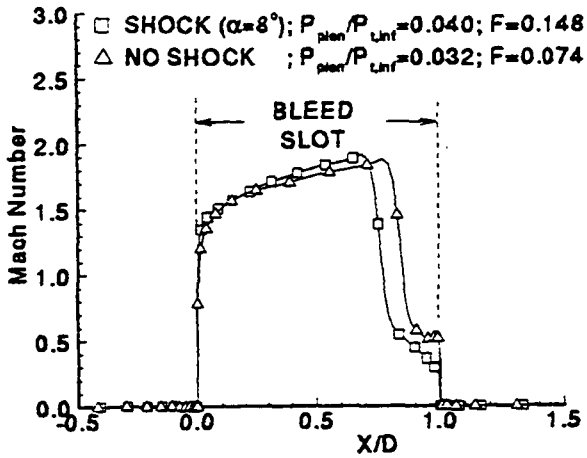

Fig. 11. Mach Number Across Slot Opening.

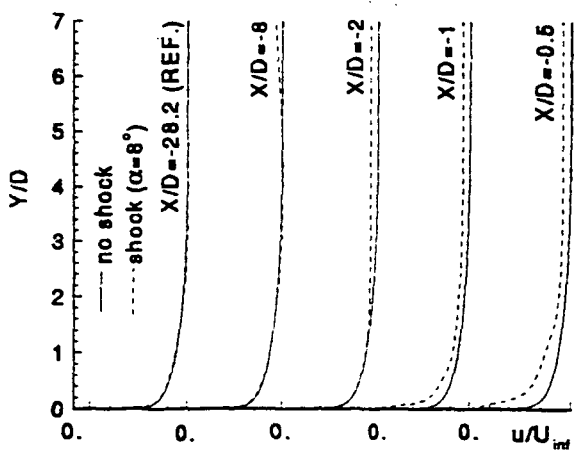

(a) Upstream of Bleed Slot

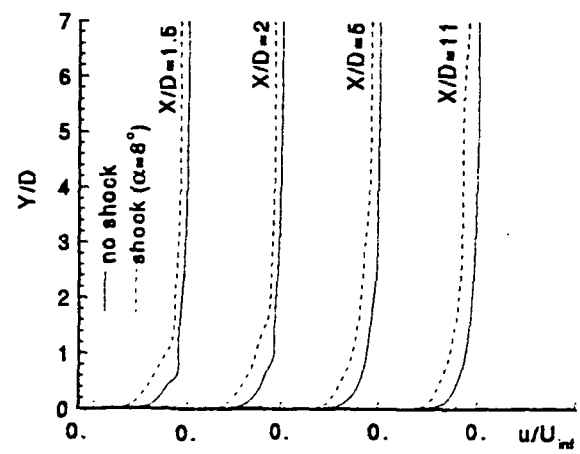

(b) Downstream of Bleed Slot

Fig. 12. Boundary Layer Velocity Profiles

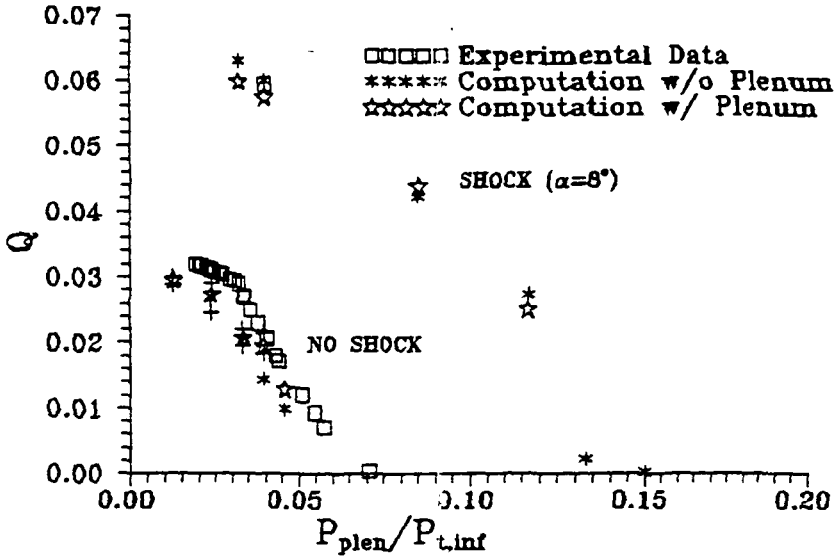

Fig. 13. Bleed Discharge Coefficient Based on $P_{t_{inf}}$

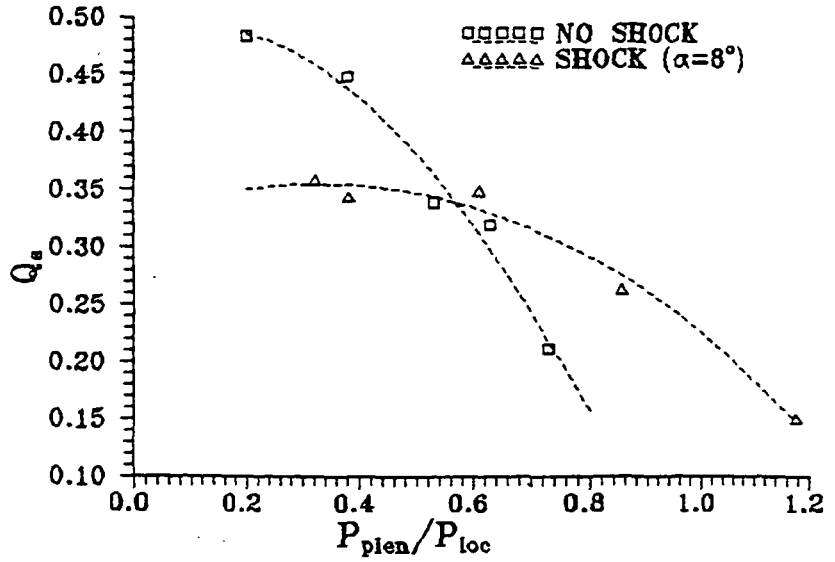

Fig. 14. Bleed Discharge Coefficient Based on P_{loc}